analytical chemistry

pubs.acs.org/ac Article

Ultrasensitive and Label-Free Detection of Multiple DNA Methyltransferases by Asymmetric Nanopore Biosensor

Siqi Zhang, Wei Shi, Kai-Bin Li, De-Man Han,* and Jing-Juan Xu

Cite This: *Anal. Chem.* 2022, 94, 4407−4416 Read Online

ACCESS | Metrics & More | Article Recommendations | Supporting Information

ABSTRACT: DNA methylation is catalyzed by a family of DNA methyltransferases that play crucial roles in various biological processes. Therefore, an ultrasensitive methyltransferase assay is highly desirable in biomedical research and clinical diagnosis. However, conventional assays for the detection of DNA methyltransferase activity often involve radioactive labeling, costly equipment, and laborious operation. In this study, an ultrasensitive and label-free method for detecting DNA adenine methyltransferase (Dam) and CpG methyltransferase (M.SssI) was developed using the nanopore technique coupled with DNA cascade signal amplification reactions. A hairpin DNA (H_D) comprising of the methylation-responsive sequences was skillfully designed. In the presence of Dam methyltransferase, the corresponding recognition site of hairpin H_D was methylated and specifically cleaved by *Dpn*I endonuclease, thus forming a DNA fragment that induces the catalytic hairpin assembly and hybridization chain reaction (CHA−HCR). The generated products could be absorbed onto the Zr^{4+}-coated nanopore, resulting in an ion current rectification signal change. Considering the high sensitivity of the nanopore and excellent specificity toward the recognition of methyltransferase/endonuclease, our developed method could detect both Dam and M.SssI methyltransferases in the same sensing platform. Furthermore, the designed nanopore sensor could realize the multiplex detection of Dam and M.SssI methyltransferases after integration with the cascaded INHIBIT−AND logic gate. This ultrasensitive methyltransferase assay holds great promise in the field of cancer diagnosis.

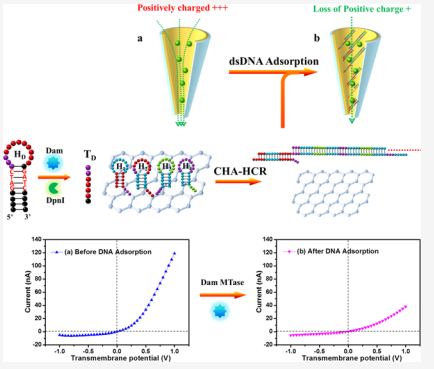

INTRODUCTION

DNA methylation is catalyzed by a family of DNA methyltransferases that participate in crucial epigenetic and biological processes in both eukaryotes and prokaryotes.[1,2] DNA methyltransferase specifically recognizes adenine/cytosine sites and transfers the methyl group from *S*-adenosylmethionine (SAM) to the target DNA sequences.[3] Abnormal DNA methylation status has been correlated to the disruption of DNA methyltransferase activities, which can lead to genetic diseases and cancers.[4] Therefore, DNA methyltransferases have been recognized as key biomarkers for early clinical diagnosis.

To date, various approaches have been proposed for detecting DNA methyltransferase activity, including high-performance liquid chromatography,[5] high-performance capillary electrophoresis,[6] polymerase chain reaction,[7] immunochemical approaches,[8] gel electrophoresis,[9] and radioactive assay.[10] However, most of the detection methods involve sophisticated detection equipment,[5,7] radio-labeled substrates,[10] specific antibodies,[8] and laborious operation.[9] Recently, several alternative methods have been established, such as fluorescent,[11,12] colorimetric,[13] electrochemical,[14] photoelectrochemical,[15,16] and chemiluminescent methods.[17] Among them, electrochemical approach has been commonly used for DNA methylation assay due to its advantages of simple operation, microminiaturization, low cost, and fast response. For instance, Gao's group[18] developed an electrochemical method for M.SssI methyltransferase detection and inhibitor screening. Barton's group[19] reported a multiplex, electrochemical chip for detecting bacterial and human methyltransferase activity. However, most electrochemical methods required tedious surface modification of the DNA probes on the electrode surfaces. To improve the sensitivity of electrochemical methods, a number of isothermal enzymatic amplification strategies have been developed, including exonuclease-assisted amplification,[14] strand-displacement-based signal amplification (SDA),[20] hybridization chain reaction (HCR),[21] and rolling circle amplification (RCA).[22] Unfortunately, the signal amplification-based electrochemical sensors often encounter the problems of local steric hindrance and limited reaction area. This in turn affects the activity of the biomolecules and the amplification efficiency of the electrochemical sensors. Therefore, it is of utmost importance to

Received: December 9, 2021
Accepted: February 21, 2022
Published: March 2, 2022

https://doi.org/10.1021/acs.analchem.1c05332
Anal. Chem. 2022, 94, 4407−4416

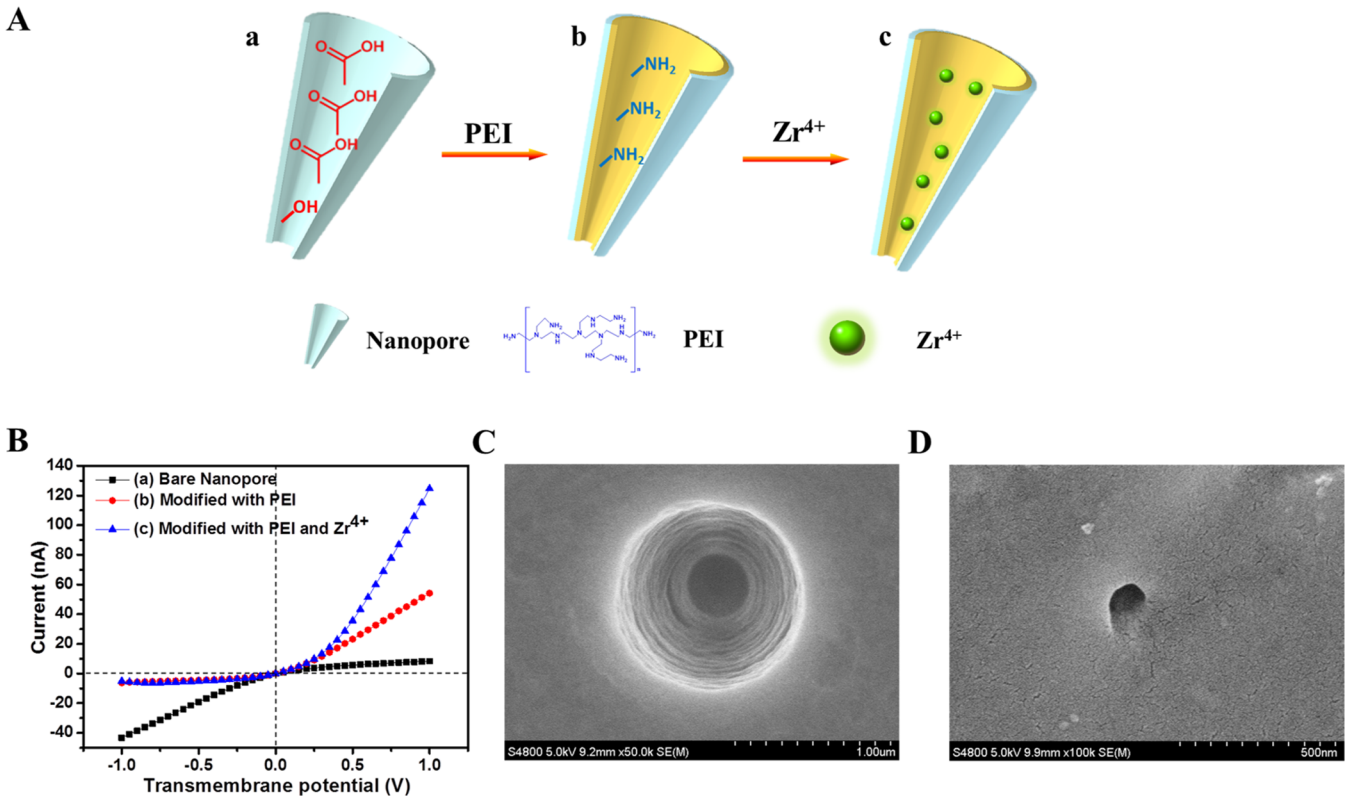

Figure 1. (A) Schematic illustration of the PEI/Zr^{4+}-functionalized nanopore. (a) Bare nanopore, (b) PEI-modified nanopore, (c) PEI and Zr^{4+}-modified nanopore. (B) Current−voltage characteristic curve of each surface modification step. Scanning electron microscopy (SEM) images of the base (C) and tip (D) sides of the nanopore.

establish a novel sensing platform for a homogeneous methyltransferase assay.

As one of the biomimetic nanodevices, nanopore sensor has attracted widespread attention and been widely developed.[23−28] The unique three-dimensional (3D) nanostructure and abundant functional groups enable the nanopore sensor to detect analytes with high sensitivity and excellent selectivity.[29,30] For instance, Xia's group[31,32] developed a nanopore sensing device for detecting DNA and ATP and realized the ultrasensitive detection of DNA by assembling a supersandwich structure in the nanopores with a limit of detection (LOD) of 10 fM. Sun's group[33] fabricated a new phosphorodiamidate morpholino oligonucleotide-modified nanopore sensing platform for the identification of miRNAs with a LOD of 10 fM in serum samples and 1 fM in phosphate-buffered saline. However, the sensing reaction of the aforementioned nanopore sensor is mainly initiated at the interface between nanopore and solution, which belongs to heterogeneous reaction. Compared with homogeneous reaction, heterogeneous reaction is relatively inefficient and difficult to control, which limits the improvement of the detection sensitivity and stability of nanopore sensing technology. Due to the existence of steric hindrance, the modification and assembly of the DNA probe onto the nanopore surface requires a lot of time, which also limits the development and application of nanopore sensors. Recently, Wang's group[34,35] and our group[36] established a novel homogeneous nanopore sensing technology for the detection of melamine/adamantanamine/miRNA. In this sensing mode, the assembly of probe and signal amplification was completed in solution, and then the product was adsorbed to the inner wall of the nanopore through an external electric field to change the nanopore surface charge and output the ion rectification signal. The new sensing mode is homogeneous and immobilization-free, which has a broad detection range and high selectivity. However, these nanopore sensors have not been deployed to detect DNA methyltransferase activity. Therefore, we aimed to develop a novel nanopore sensor for detecting methyltransferase activity.

Herein, a simple and novel nanopore sensor in combination with cascade signal amplification was constructed to detect methyltransferase activity and screen methyltransferase inhibitors. Considering the specific recognition of methyltransferase/endonuclease, the concatenated catalyzed hairpin DNA (H_D) assembly and hybridization chain reaction (CHA−HCR) was triggered and the assembled product (double-stranded DNA (dsDNA)) was adsorbed onto the surface of the nanopore modified with Zr^{4+}. The corresponding surface charge of the nanopore sensor was changed, which could be detected by ion current rectification (ICR). Thus, the homogeneous nanopore sensing platform could serve as an ultrasensitive and rapid detection method for the methyltransferase assays (Dam and M.SssI methyltransferase). Moreover, the proposed nanopore sensor could be used to construct different logic gates. It was found that Dam and M.SssI methyltransferase could be differentiated and detected through the use of combinational logic gates (AND and INHIBIT).

EXPERIMENTAL SECTION

Conical Nanochannel Fabrication. A single conical nanochannel was prepared on a 12 μm poly(ethylene

https://doi.org/10.1021/acs.analchem.1c05332
Anal. Chem. 2022, 94, 4407−4416

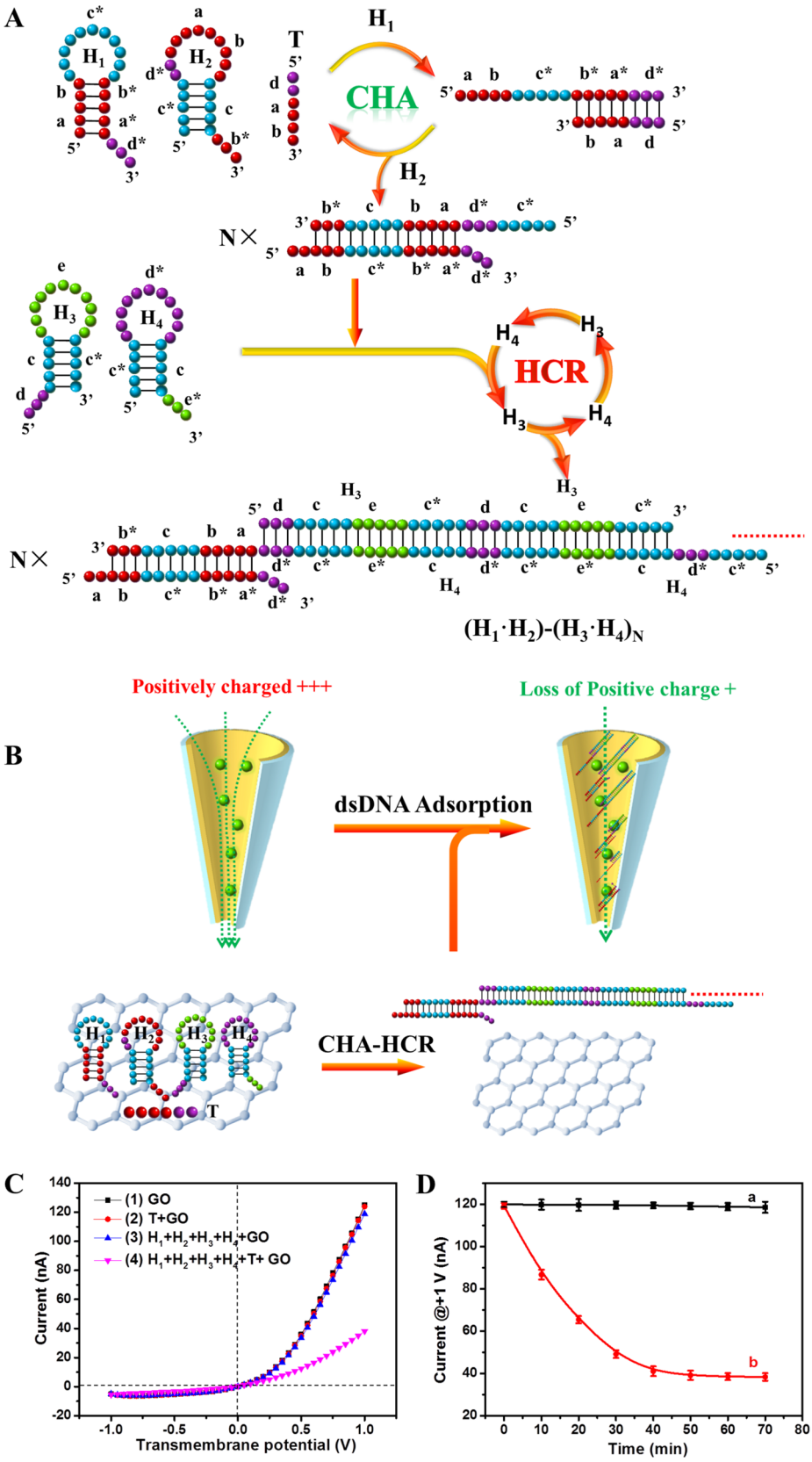

Figure 2. (A) Scheme of the CHA−HCR cascade amplification system. (B) Illustration of the sensing strategy based on Zr^{4+}-coated nanopore for the initiator sequence (T). (C) Current−voltage curves of the Zr^{4+}-coated nanopore in the presence of GO (1), GO + 10 nM T (2), GO + 500 nM H_1−H_4 (3), and GO + 500 nM H_1−H_4 + 10 nM T (4). Transmembrane current measurement was conducted after 1 h. (D) Variations in current@ + 1V with the time of the CHA−HCR system in the presence of GO + 500 nM H_1−H_4 (a) and GO + 500 nM H_1−H_4 + 10 nM T (b).

https://doi.org/10.1021/acs.analchem.1c05332
Anal. Chem. 2022, 94, 4407−4416

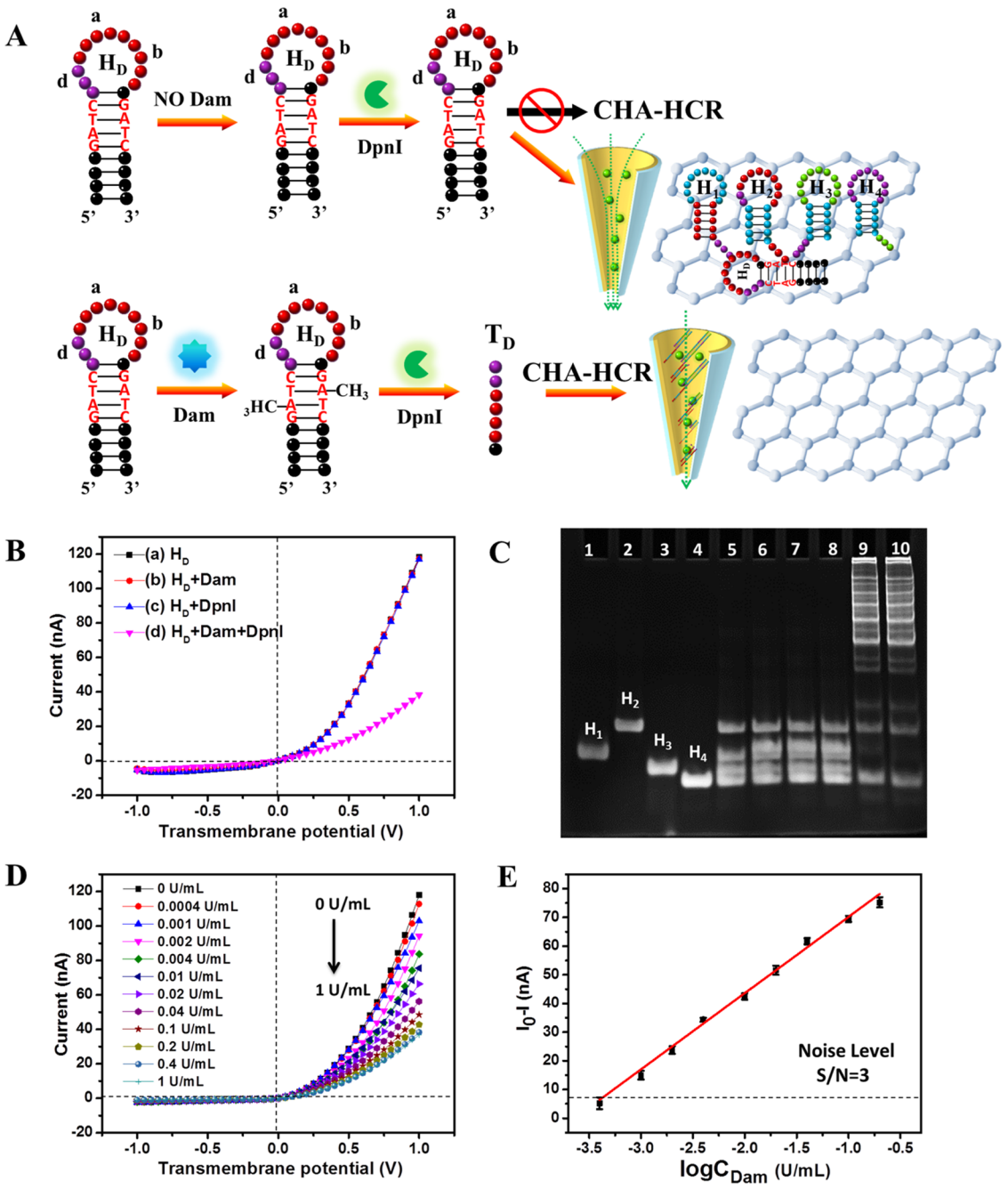

Figure 3. (A) Scheme for the CHA−HCR-motivated Dam methyltransferase assay. (B) Current−voltage curves of the CHA−HCR system after adding H_D (a), H_D + Dam methyltransferase (b), H_D + *Dpn*I (c), and H_D + Dam methyltransferase + *Dpn*I (d). The final concentrations of Dam methyltransferase and *Dpn*I were 1.0 and 40 U/mL, respectively. (C) PAGE analysis of the CHA−HCR-motivated Dam methyltransferase detection: (1) H_1, (2) H_2, (3) H_3, (4) H_4, (5) H_1−H_4, (6) H_1−H_4, H_D, (7) H_1−H_4, H_D, and Dam methyltransferase, (8) H_1−H_4, H_D, and *Dpn*I, (9) H_1−H_4, H_D, Dam methyltransferase, and *Dpn*I, and (10) H_1−H_4 and T. (D) Current−voltage curves of the CHA−HCR system incubated with various concentrations of Dam methyltransferase. (E) Linear calibration curve of the CHA−HCR-motivated Dam methyltransferase assay, as plotted by ionic current change ($I - I_0$) versus Dam methyltransferase concentration.

terephthalate) (PET) membrane using the track-etch technique. Prior to chemical etching, all sides of the PET membrane were subjected to UV irradiation at 365 nm for 1 h. The PET membrane was sandwiched between two chambers of a custom-built etching cell, in which one chamber comprised of 6 M NaOH (etching solution) and another one of 1 M HCOOH + 1 M KCl (stopping solution) at 60 °C. The etching process was monitored by a platinum electrode pair with a 1 − V voltage across the membrane. The etching was terminated when the current achieved the desired value, and the membrane was immersed in the water quickly to remove salt residues. Multitrack (1×10^6 tracks/cm^2) PET membranes were also etched by the same operating procedure. The tip and base diameters of the nanopore were measured using a field emission scanning electron microscope. As demonstrated in Figure 1C,D, the tip diameter of the nanopore was 85 nm, while the base diameter of the nanopore was 1.14 μm (Figure 1C,D). After chemical etching, the hydroxy and

https://doi.org/10.1021/acs.analchem.1c05332
Anal. Chem. 2022, 94, 4407−4416

carboxyl groups were generated on the surface of the nanopore. The membrane was modified with polyethyleneimine (PEI) by immersing it in 1% PEI for 10 h and electrostatic attraction onto the nanopore surface. Next, the tip side of the nanopore was incubated with zirconium acetate (8 wt % aqueous solution) for 30 min.

Dam Methyltransferase Assay. Dam methyltransferase assay was conducted in 50 μL of Dam methyltransferase reaction buffer (supplied by NEB). Two microliters H_D (2 μM) were mixed with 5 μL of SAM (1600 μM), 40 U/mL *Dpn*I, 5 μL of Cutsmart Buffer (10×), and various concentrations of Dam methyltransferase, followed by incubation for 2 h at 37 °C. The Dam/*Dpn*I-treated solution was subsequently added with hairpin DNA H_1−H_4 (500 nM each) to initiate the homogeneous CHA−HCR reaction at 37 °C for 1 h. Next, 100 μL of graphene oxide (GO) (500 μg/mL) were placed in the centrifuge tube and reacted for 30 min. Afterward, the Tris−HCl buffer was used to dilute the resulting solution to 1 mL. Lastly, the product solution was transferred onto the tip side of the nanopore, and the current−voltage curves were obtained by scanning voltages (range: −1.0 to +1.0 V). Similarly, the process of M.SssI methyltransferase assay is illustrated in the Supporting Information.

RESULTS AND DISCUSSION

Surface Modification of the Nanopore. At the initial stage, the −COOH and −OH groups were produced on the nanopore surface due to the chemical etching of the nanopore in the PET membrane. When the nanopore was exposed to a neutral solution, the deprotonated carboxyl and hydroxy groups could cause the nanopore surface to be negatively charged (Figure 1A(a)). Next, the transmembrane ionic current was measured to confirm the surface modification process. The ion current rectification (ICR) curves are displayed in Figure 1B. As discussed above, the bare conical nanopore was negatively charged, and a downward shape was observed in the ICR curve (Figure 1B(a)). After modifying the positively charged PEI, the ICR curve showed an upward shape (Figure 1B(b)). This is because the protonation of the amino groups in PEI causes the nanopore surface to become positively charged. Subsequently, the positively charged Zr^{4+} was absorbed onto the nanopore surface and enhanced the ICR signal of the nanopore due to the accumulation of positive charges (Figure 1B(c)).

Realization of CHA−HCR Cascade Amplification Strategy. As illustrated in Figure 2A, an autonomous CHA−HCR cascade reaction was developed for signal amplification. The CHA−HCR circuit was composed of CHA (H_1−H_2) and HCR (H_3−H_4). The initiator sequence (T) was specifically designed and could trigger the CHA−HCR reaction. The initiator sequence (T) first hybridized with the hairpin probe H_1 and opened the hairpin structure. The complex T−H_1 exposed the domain a−b−c*, which served as a toehold to bind with the probe H_2. The entropy-driven T-catalyzed hairpin assembly triggered the hybridization between H_1 and H_2 for multiple cycles, thus resulting in the continuous production of H_1−H_2 duplex. The fragment c*−d* of H_2 was exposed and might serve as a new primer to motivate the subsequent HCR process. The exposed fragment c*−d* hybridized with H_3 and opened H_3 to expose the fragment e−c* to bind with H_4. The opened H_4 exposed the fragment c*−d* and motivated the next cycle of HCR. Thus, the HCR reaction could be successively accelerated from the CHA reaction, which in turn assembled the dsDNA nanowires in the solution.

The CHA−HCR system was used in the nanopore sensing platform (Figure 2B). According to the previous literature,[37] graphene oxide (GO) could absorb the single-stranded DNA (ssDNA) and hairpin DNA but not double-stranded DNA. Thus, GO was utilized to remove the excess single-stranded DNA (ssDNA) and hairpin DNA, which had not yet folded into a duplex conformation. In the absence of the initiator sequence (T), the hairpins H_1−H_4 could coexist metastably and be absorbed onto the GO surface, leading to no free DNA probes in the solution. Hence, the DNA probes could not be absorbed onto the Zr^{4+}-coated nanopore and the surface charge of the nanopore remained unchanged. As shown in Figure 2C (curve 3), the corresponding ICR signal did not change before adding the initiator sequence (T). In the presence of the initiator sequence (T), the initiator sequence (T) could trigger the CHA−HCR reaction and produce numerous dsDNA nanowires, which were easily detached from the GO surface and absorbed onto the nanopore surface. As a result, the positive charge of the nanopore surface was neutralized by dsDNA nanowires. GO acted as an absorbent material to remove the excess and unreacted DNA probes, which could reduce the background signal caused by the nonspecific adsorption of DNA probes. As shown in Figure 2C (curve 4), a significant change in the ICR signal could be obtained due to the CHA−HCR reaction. The ICR signal reached rock bottom after 1 h (Figure 2D, curve b). As expected, the initiator sequence (T) could trigger the CHA−HCR system and be detected by the ICR signal, suggesting that the homogeneous CHA−HCR system could be applied for methyltransferase activity detection and methyltransferase inhibition. Polyacrylamide gel electrophoresis (PAGE) was also used to clarify the mechanism of the CHA−HCR reaction. Obviously, the initiator sequence (T) could trigger both CHA and CHA−HCR reactions (Figure S1).

Application of the CHA−HCR System for Dam Methyltransferase Assay. By virtue of the high signal amplification and widespread application of the CHA−HCR reaction, the proposed cascade amplification system was applied to detect Dam methyltransferase and its inhibitors. Figure 3A delineates the principle of the CHA−HCR-involved Dam methyltransferase assay. Hairpin H_D was designed with symmetric tetranucleotide 5′-G-A-T-C-3′ that can be recognized by *Dpn*I and Dam methyltransferase. The recognizable sequences were embedded in the stem region of H_D. The triggered sequences were locked in the loop region and partial stem region of H_D and could be released to initiate the CHA−HCR system in the presence of *Dpn*I/Dam methyltransferase. Without Dam methyltransferase, the endonuclease *Dpn*I could not cleave the nicking domain of H_D owing to the absence of the 5′-G-A-T-C-3′ methylation site. Hence, the hairpin H_D was intact and CHA−HCR-triggered sequences were still locked in H_D substrate. The subsequent CHA−HCR was prohibited and the nanopore surface charge remained unchanged. Dam methyltransferase catalyzed the transfer of a methyl group from SAM to the N6 position of an adenine residue within the H_D recognition site, thus producing the methylated sequence 5′-G-mA-T-C-3′. Subsequently, *Dpn*I could cleave the nicking domain of H_D, release the triggered sequence (T_D) to initiate the CHA−HCR system, and change the nanopore surface charge as described above. The ionic current measurement was conducted to demonstrate the feasibility of the CHA−HCR-

https://doi.org/10.1021/acs.analchem.1c05332
Anal. Chem. 2022, 94, 4407−4416

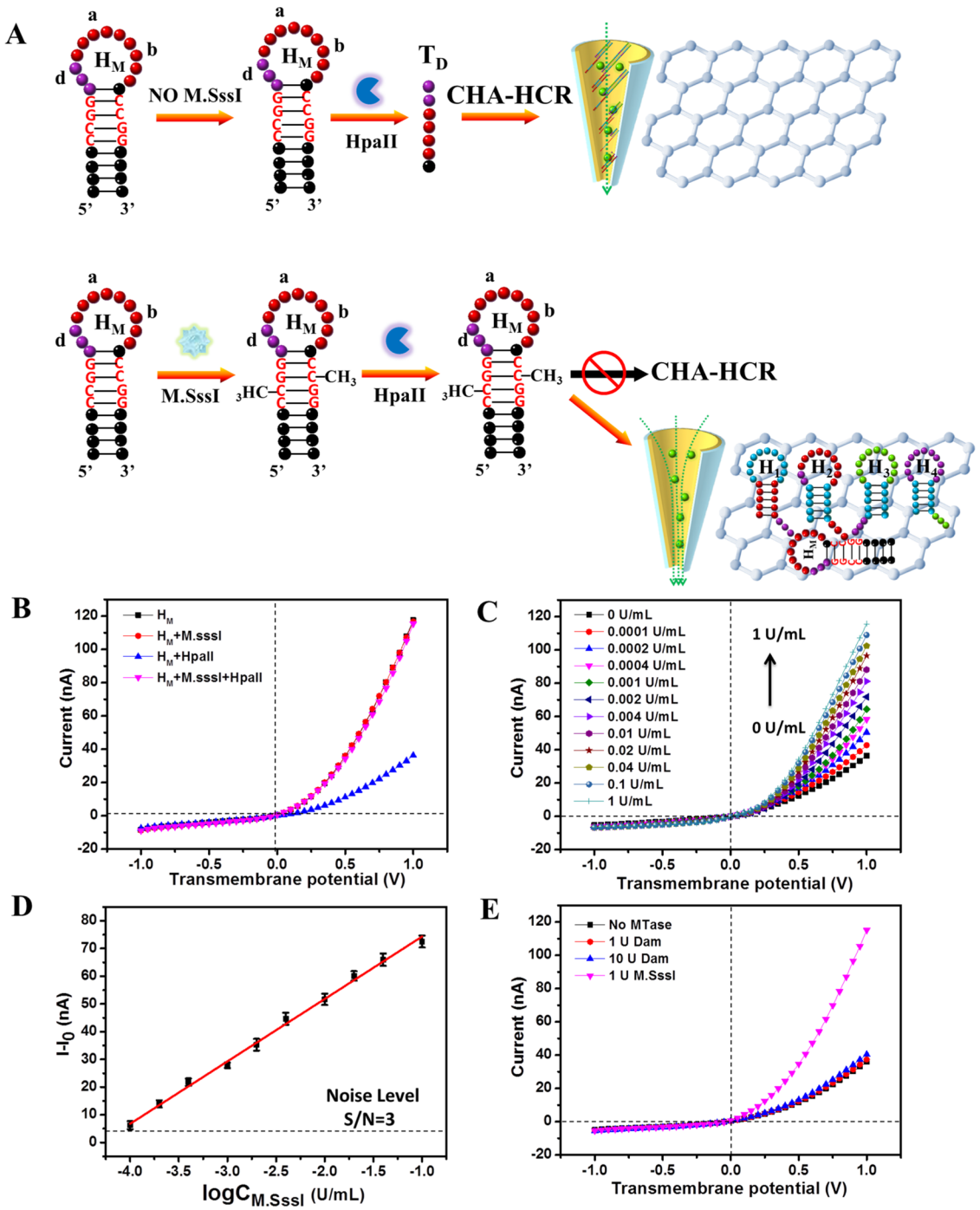

Figure 4. (A) Schematic for the CHA−HCR-motivated M.SssI methyltransferase assay. (B) Current−voltage curves of the CHA−HCR system after adding H_M (a), H_M + M.SssI methyltransferase (b), H_M + *Hpa*II (c), and H_D + M.SssI methyltransferase + *Hpa*II (d). Final concentrations of M.SssI methyltransferase and *Hpa*II were 1 and 20 U/mL, respectively. (C) Current−voltage curves of the CHA−HCR system incubated with varying concentrations of M.SssI methyltransferase. (D) The corresponding linear calibration curves of the CHA−HCR-motivated M.SssI methyltransferase assay, as plotted by ionic current change ($I - I_0$) versus M.SssI methyltransferase concentration. (E) Current−voltage curves of the CHA−HCR system after exposure to blank, M.SssI methyltransferase (1 U/mL), and Dam methyltransferase (1 and 10 U/mL).

motivated Dam methyltransferase assay (Figure 3B). As expected, no obvious ionic current change was observed between *Dpn*I-treated H_D and untreated H_D since the methylation of H_D did not occur without Dam methyltransferase. The *Dpn*I endonuclease could not cleave the unmethylated sequences and no CHA−HCR reaction occurred, leading to no change in the surface charge of the nanopore (curves a and c in Figure 3B). In the presence of *Dpn*I and Dam methyltransferase, the signal amplification was remarkably decreased (Figure 3B, curve d), implying the methylation of H_D and the subsequent cleavage of the methylated H_D (Figure 3A). Additionally, in the absence of *Dpn*I endonuclease, a negligible ionic current change was observed, demonstrating that the cleavage of the methylated H_D was accomplished by *Dpn*I endonuclease (curve b in Figure 3B).

https://doi.org/10.1021/acs.analchem.1c05332
Anal. Chem. 2022, 94, 4407−4416

Moreover, PAGE was performed to characterize the CHA−HCR-motivated Dam methyltransferase assay (Figure 3C). Lanes 1−4 show the belt locations of H_1, H_2, H_3, and H_4, respectively. No new band was observed in the mixture of H_1−H_4 (lane 5) and the mixture of H_1−H_4 and H_D (lane 6), indicating that the hairpins could coexist in the system. When Dam methyltransferase was introduced into the mixture of H_1−H_4 and H_D, no new band appeared in lane 7, as the biosensing system might lack the corresponding endonuclease. Similarly, when only *Dpn*I endonuclease was introduced into the mixture of H_1−H_4 and H_D, no new band was observed, implying that *Dpn*I could not cleave the unmethylated H_D and thus the CHA−HCR biosensing system was not initiated. However, a large number of new bands appeared when Dam methyltransferase and *Dpn*I were simultaneously added into the biosensing system (lane 9). This phenomenon was the same as that of the initiator sequence (T)-triggered CHA−HCR system (lane 10), indicating only the methylated H_D could be cleaved by *Dpn*I endonuclease and motivate the CHA−HCR reaction. These gel electrophoresis results were consistent with the previous ionic current measurement (Figure 3B), verifying that the CHA−HCR system could accurately detect *Dpn*I and Dam methyltransferase activities.

Analytical Performance of Dam Methyltransferase Assay. The *Dpn*I concentration and reaction time were optimized to achieve the best performance for the methyltransferase assay (Figure S5). The optimal *Dpn*I concentration and methylation/cleavage time were 40 U/mL and 2 h, respectively. The sensing performance of Dam methyltransferase was further evaluated by monitoring the current−voltage curves of the CHA−HCR system after adding various concentrations of Dam methyltransferase. As shown in Figure 3D, the ICR curve of Zr^{4+}-coated nanopore gradually flattened with the increasing Dam methyltransferase concentrations, since the positive charge of the nanopore surface was neutralized by the dsDNA nanowires. Hence, the calibration curve method could be applied to determine the concentration of Dam methyltransferase.

The ion current change ($I_0 - I$) was used to characterize the ion current change value at +1.0 V. The ion current change generally increased at Dam methyltransferase concentration range of 0.0004−1.0 U/mL. I and I_0 represent the corresponding ionic currents after exposure to a solution containing Dam methyltransferase and control solution (0 U/mL Dam methyltransferase), respectively. As shown in Figure 3E, a series of ion current changes ($I_0 - I$) was gained. A good linear relationship between $I_0 - I$ and the logarithm of Dam methyltransferase (range: 0.0004−0.4 U/mL) was derived from the following linear regression equation: $I_0 - I$ (nA) = 96.7524 + 26.5693 log C_{Dam} (R^2 = 0.9927). The noise signal was calculated by repeatedly measuring the blank solutions without Dam methyltransferase seven times. A dotted line in Figure 3E indicates the value of a threefold noise. The LOD was calculated as 0.001 U/mL since the signal of 0.001 U/mL exceeded the background noise by 3 times. The LOD was relatively lower than that reported for most Dam methyltransferase sensors (Table S2).

Evaluation of the Selectivity of Dam Methyltransferase Activity and Its Inhibitors. The selectivity of Dam methyltransferase activity assay was further evaluated by introducing M.SssI methyltransferase as an interfering methyltransferase control. M.SssI methyltransferase could transfer a methyl group from SAM to the cytosine residues within the 5′-G-C-3′ recognition site. As demonstrated in Figure S2A,B, a significant ion current change was detected at 1 U/mL Dam methyltransferase, while a negligible ion current change was obtained by introducing a 10-fold concentration of M.SssI methyltransferase. Hence, the proposed CHA−HCR system shows excellent performance in distinguishing Dam methyltransferase from other methyltransferases owing to the unique recognition sequences of methyltransferase/endonuclease.

Previous research had shown that abnormal methylation level was associated with a wide variety of human diseases. Therefore, methyltransferase inhibitor screening holds a great promise for early cancer diagnosis. Herein, gentamycin sulfate (an antibiotic) and 5-fluorouracil (an anticancer drug) were selected as the model inhibitors on Dam methyltransferase. Upon the addition of gentamycin sulfate and 5-fluorouracil, a significant ion current change was observed (Figure S2C), indicating that these Dam methyltransferase inhibitors might inhibit the methylation of H_D. Between these two inhibitors, 5-fluorouracil exhibited more effective inhibitory effects compared with gentamycin sulfate. In addition, the concentration-dependent inhibitory effect of 5-fluorouracil was further investigated (Figure S2D). The ion current change of the sensing system reduced gradually with the increasing concentrations of 5-fluorouracil (range: 0−5 μM), and the IC_{50} value of 5-fluorouracil reached as high as 3 μM. These results indicated that our CHA−HCR-motivated strategy for screening methyltransferase inhibitors could be extended to assess the inhibitory effects of different therapeutic agents on Dam methyltransferase activity.

Analytical Performance of M.SssI Methyltransferase Assay. The established CHA−HCR-motivated methyltransferase assay was applied to detect M.SssI methyltransferase activity by changing the hairpin sequence. H_M was designed with symmetric tetranucleotide 5′-C-C-G-G-3′ in the stem region, which could be recognized by *Hpa*II and M.SssI methyltransferase (Figure 4A). As a result, the trigger sequences could also be released to initiate the CHA−HCR system through *Hpa*II endonuclease. Different from Dam methyltransferase/*Dpn*I system, the CpG dinucleotide site of 5′-C-C-G-G-3′ was not methylated without M.SssI methyltransferase. *Hpa*II could cleave the hairpin H_M, thereby releasing the triggered sequence (T_M) to initiate the CHA−HCR system and changing the nanopore surface charge as described before (curve c in Figure 4B). On the contrary, M.SssI methyltransferase catalyzed the methylation of CpG dinucleotides, and *Hpa*II could not cleave the methylated H_M, thus blocking the CHA−HCR reaction. As a result, the nanopore surface charge and the ion current signal remained unchanged (curve d in Figure 4B). Similar to Dam methyltransferase assay, the analytical performance of M.SssI methyltransferase assay was also investigated by measuring the current−voltage curves for various concentrations of M.SssI methyltransferase and a constant concentration of *Hpa*II endonuclease. With increasing M.SssI methyltransferase concentrations, the ICR curve showed a gradual upward trend (Figure 4C), since M.SssI methyltransferase catalyzed the methylation of H_M and *Hpa*II cleavage was prohibited. The calibration curve method was employed to determine the concentrations of M.SssI methyltransferase. The ion current change ($I - I_0$) was used to characterize the ion current change value at +1.0 V. The ion current change generally increased with increasing M.SssI methyltransferase concentrations

https://doi.org/10.1021/acs.analchem.1c05332
Anal. Chem. 2022, 94, 4407−4416

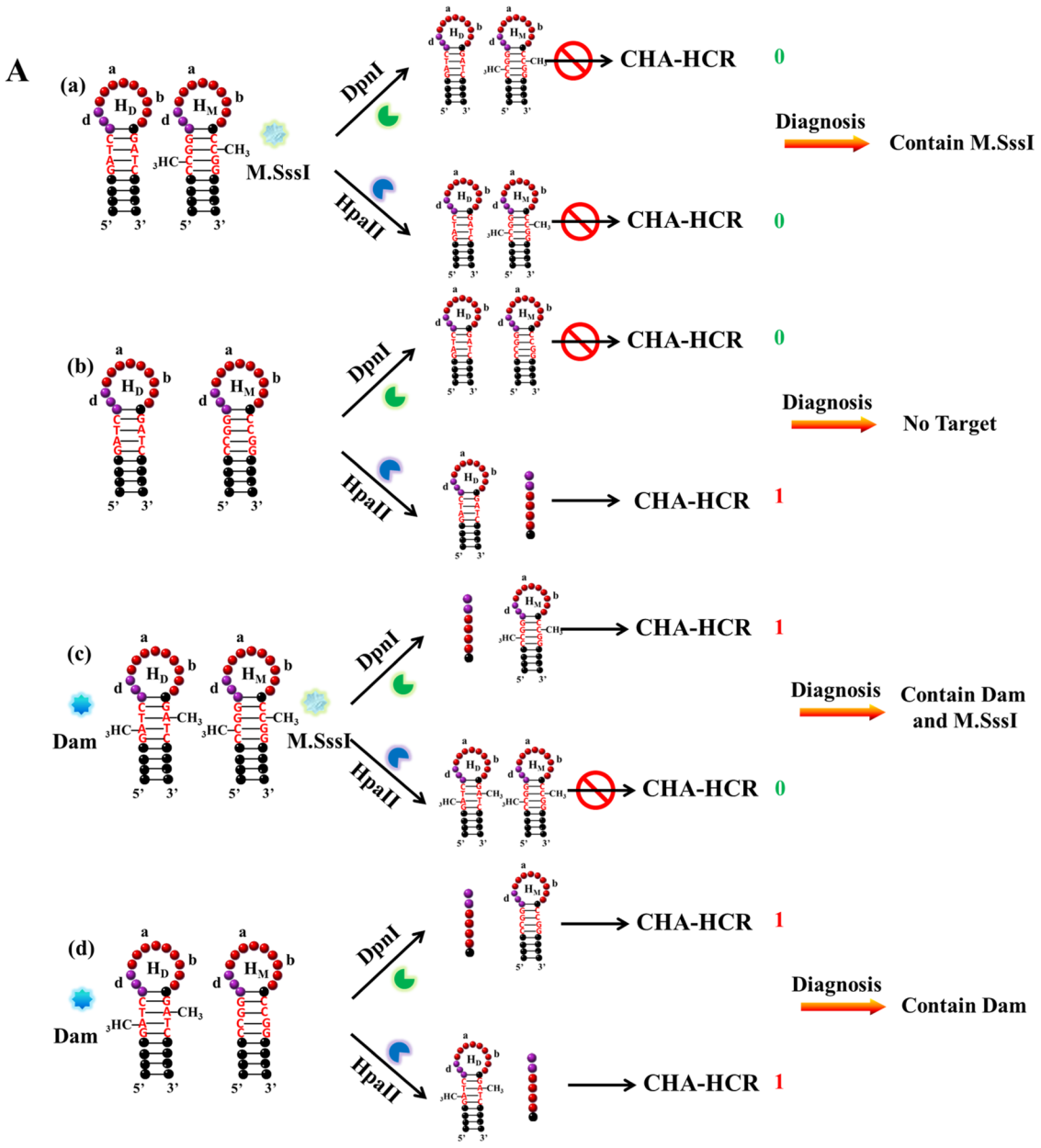

B

sample		I	II	Diagnosis
Inputs	DpnI	1	0	
	HpaII	0	1	
Outputs	a	0	0	Contain M.SssI
	b	0	1	No Target
	c	1	0	Contain Dam and M.SssI
	d	1	1	Contain Dam

Figure 5. (A) Schematic of the multiplexed analysis of Dam and M.SssI methyltransferases in samples I and II. (B) Truth table of the cascaded INH−AND logic gates.

(range: 0.0001−1.0 U/mL). I and I_0 are the corresponding ionic currents after exposure to M.SssI methyltransferase-containing solution and control solution (0 U/mL M.SssI methyltransferase), respectively. Figure 4D shows a good linear correlation between $I - I_0$ and the logarithm of M.SssI methyltransferase (range: 0.0001−0.1 U/mL). The equation for the linear correlation was as follows: $I_0 - I$ (nA) = 96.8447 + 22.5185 log $C_{M.SssI}$ (R^2 = 0.9957). Furthermore, the LOD was 0.0001 U/mL, since the signal caused by 0.0001 U/mL exceeded the background noise by 3 times. The LOD of M.SssI methyltransferase assay was lower than that of previously reported methods (Table S3). The selectivity of M.SssI methyltransferase assay was also examined using Dam methyltransferase as an interfering methyltransferase control.

https://doi.org/10.1021/acs.analchem.1c05332
Anal. Chem. 2022, 94, 4407−4416

Notably, a significant signal increase was observed for 1 U/mL M.SssI methyltransferase when compared to no methyltransferase as well as 1 and 10 U/mL Dam methyltransferase (Figure 4E). This might be attributed to the fact that M.SssI methyltransferase completely methylated the hairpin H_M and prevented H_M from being cleaved by *Hpa*II endonuclease. Hence, the CHA−HCR system could not be motivated and the surface charge of the nanopore remained unchanged. These results indicated that M.SssI methyltransferase could be distinguished from other methyltransferases in the CHA−HCR-motivated methyltransferase assay due to the specific recognition sequences of H_M.

Multiplexed Analysis of Dam and M.SssI Methyltransferases under Cascaded INH−AND Logic Control. The proposed CHA−HCR-motivated methyltransferase assay was applied to build logic circuits. As shown in Figure S3, an analog AND gate was constructed using the biosensing system, where Dam methyltransferase and *Dpn*I endonuclease were required to trigger the CHA−HCR reaction. To evaluate the application of the CHA−HCR-motivated methyltransferase assay in intelligent analyte detection, the INHIBIT logic gate was also constructed (Figure S4).

The integration of AND and INHIBIT logic gates served as a promising method for detecting multiple DNA methyltransferases (Dam and M.SssI). Based on the ionic current signal output, the presence of Dam methyltransferase or M.SssI methyltransferase could be logically judged. As shown in Figure 5A, different samples were inputted to the CHA−HCR biosensing system ($H_D/H_M/H_{1-4}$). The detection system was divided into two separate samples, namely, sample I and sample II. Next, *Dpn*I and *Hpa*II were added into the two biosensing systems (sample I and sample II), respectively. If no obvious signal changes were detected in both samples, then the sample was considered to consist of M.SssI methyltransferase but not Dam methyltransferase (see item a in Figure 5A). This was because *Dpn*I could not cleave H_D in the absence of Dam methyltransferase, whereas *Hpa*II could not cleave H_M in the presence of M.SssI methyltransferase. The CHA−HCR reaction could not be initiated under these situations. If there was an obvious signal change in sample II but not in sample I, no methyltransferases were detected in the sample (see item b in Figure 5A). This was because *Dpn*I could not cleave H_D in the absence of Dam methyltransferase, whereas *Hpa*II could cleave H_M in the absence of M.SssI methyltransferase. Thus, the CHA−HCR reaction was not motivated in sample I, but instead motivated in sample II. If an obvious signal change was only observed in sample I, then the sample was considered to consist of both Dam and M.SssI methyltransferases (see item c in Figure 5A). This was because *Dpn*I could cleave H_D in the presence of Dam methyltransferase, while *Hpa*II could not cleave H_M in the presence of M.SssI methyltransferase. Thus, the CHA−HCR reaction was motivated in sample I but not in sample II. If obvious signal changes were observed in both samples, it indicated that the sample contained only Dam methyltransferase (see item d in Figure 5A). This was because *Dpn*I could cleave H_D in the presence of Dam methyltransferase, while *Hpa*II could cleave H_M in the absence of M.SssI methyltransferase. As a result, the CHA−HCR reaction was initiated in both samples. The truth table of the multiplexed analysis of Dam and M.SssI methyltransferases is shown in Figure 5B, and the corresponding ionic current changes are presented in Figure S6. Based on the aforementioned analysis, the nanopore sensor was proved to be excellent for detecting multiple DNA methyltransferases under the cascaded AND and INHIBIT logic gate controls, which could hold great promise in early cancer diagnosis.

CONCLUSIONS

A label-free nanofluidic device was developed based on a CHA−HCR cascade circuit for the intelligent detection of DNA methyltransferases as well as the evaluation of its inhibitors. Our method was carried out in the homogeneous solution phase under isothermal conditions, which eliminated the complex process of DNA probe modification on the nanopore surface. The sensing mode was simple, label-free, and rapid. The proposed method also had a broad detection range and high selectivity. The LOD of 0.001 U/mL was obtained for Dam methyltransferase and 0.0001 U/mL for M.SssI methyltransferase, which was lower than that of most of the existing methyltransferase sensors. Furthermore, the proposed CHA−HCR-motivated methyltransferase assay was used to construct INHIBIT−AND logic circuits, which served as a supporting method to confirm the presence of Dam or M.SssI methyltransferase. This nanopore sensor offers a novel and interesting means for the accurate detection of multiple DNA methyltransferases, which in turn contributes to early diagnosis and drug screening.

ASSOCIATED CONTENT

Supporting Information

The Supporting Information is available free of charge at https://pubs.acs.org/doi/10.1021/acs.analchem.1c05332.

DNA sequences, optimization of *Dpn*I/*Hpa*II concentration and reaction time, native PAGE analysis, changes in the ionic current of combinatorial logic gates, and regeneration of biomimetic nanopore and comparison with other detection methods (PDF)

AUTHOR INFORMATION

Corresponding Author

De-Man Han − *School of Pharmaceutical and Materials Engineering, Taizhou University, Jiaojiang 318000 Zhejiang, China;* orcid.org/0000-0003-1995-0770; Phone: 86-576-88660353; Email: hdmtzc@126.com

Authors

Siqi Zhang − *School of Pharmaceutical and Materials Engineering, Taizhou University, Jiaojiang 318000 Zhejiang, China*

Wei Shi − *School of Pharmaceutical and Materials Engineering, Taizhou University, Jiaojiang 318000 Zhejiang, China*

Kai-Bin Li − *School of Pharmaceutical and Materials Engineering, Taizhou University, Jiaojiang 318000 Zhejiang, China*

Jing-Juan Xu − *State Key Laboratory of Analytical Chemistry for Life Science and Collaborative Innovation Center of Chemistry for Life Sciences, School of Chemistry and Chemical Engineering, Nanjing University, Nanjing 210023, China;* orcid.org/0000-0001-9579-9318

Complete contact information is available at: https://pubs.acs.org/10.1021/acs.analchem.1c05332

Notes

The authors declare no competing financial interest.

https://doi.org/10.1021/acs.analchem.1c05332
Anal. Chem. 2022, 94, 4407−4416

■ ACKNOWLEDGMENTS

This work was supported by the National Natural Science Foundation of China (Nos. 21904093 and 21976129), the Zhejiang Province Public Welfare Technology Application Research Project (No. LGF22B050001), and the Zhejiang Provincial Natural Science Foundation of China (Nos. LY22B050002 and LY22B060001).

■ REFERENCES

(1) Reik, W.; Dean, W.; Walter, J. *Science* **2001**, *293*, 1089−1093.
(2) Wolffe, A. P.; Matzke Marjori, A. *Science* **1999**, *286*, 481−486.
(3) Smith, Z. D.; Meissner, A. *Nat. Rev. Genet.* **2013**, *14*, 204−220.
(4) Choy, J. S.; Wei, S.; Lee, J. Y.; Tan, S.; Chu, S.; Lee, T.-H. *J. Am. Chem. Soc.* **2010**, *132*, 1782−1783.
(5) Lopez Torres, A.; Yanez Barrientos, E.; Wrobel, K.; Wrobel, K. *Anal. Chem.* **2011**, *83*, 7999−8005.
(6) Fraga, M. F.; Rodríguez, R.; Cañal, M. J. *Electrophoresis* **2000**, *21*, 2990−2994.
(7) Ogino, S.; Kawasaki, T.; Brahmandam, M.; Cantor, M.; Kirkner, G. J.; Spiegelman, D.; Makrigiorgos, G. M.; Weisenberger, D. J.; Laird, P. W.; Loda, M.; Fuchs, C. S. *J. Mol. Diagn.* **2006**, *8*, 209−217.
(8) Boye, E.; Marinus, M. G.; Løbner-Olesen, A. *J. Bacteriol.* **1992**, *174*, 1682−1685.
(9) Rebeck, G. W.; Samson, L. *J. Bacteriol.* **1991**, *173*, 2068−2076.
(10) Kim, B. Y.; Kwon, O. S.; Joo, S. A.; Park, J. A.; Heo, K. Y.; Kim, M. S.; Ahn, J. S. *Anal. Biochem.* **2004**, *326*, 21−24.
(11) Zhang, Y.; Wang, X. Y.; Zhang, Q. Y.; Zhang, C. Y. *Anal. Chem.* **2017**, *89*, 12408−12415.
(12) Li, C.; Wang, H.; Shang, J.; Liu, X.; Yuan, B.; Wang, F. *ACS Sens.* **2018**, *3*, 2359−2366.
(13) Liu, P.; Zhang, K. X.; Zhang, R. R.; Yin, H. S.; Zhou, Y. L.; Ai, S. Y. *Anal. Chim. Acta* **2016**, *920*, 80−85.
(14) Li, W.; Liu, X. J.; Hou, T.; Li, H. Y.; Li, F. *Biosens. Bioelectron.* **2015**, *70*, 304−309.
(15) Hou, T.; Xu, N. N.; Wang, W. X.; Ge, L.; Li, F. *Biosens. Bioelectron.* **2019**, *141*, No. 111395.
(16) Meng, L.; Xiao, K.; Zhang, X.; Du, C.; Chen, J. *Biosens. Bioelectron.* **2020**, *150*, No. 111861.
(17) Bi, S.; Zhao, T. T.; Luo, B. Y.; Zhu, J. J. *Chem. Commun.* **2013**, *49*, 6906−6908.
(18) Deng, H.; Yang, X.; Yeo, S. P. X.; Gao, Z. *Anal. Chem.* **2014**, *86*, 2117−2123.
(19) Muren, N. B.; Barton, J. K. *J. Am. Chem. Soc.* **2013**, *135*, 16632−16640.
(20) Wang, L.-j.; Han, X.; Li, C.-c.; Zhang, C.-y. *Chem. Sci.* **2018**, *9*, 6053−6061.
(21) Peng, X.; Zhu, J.; Wen, W.; Bao, T.; Zhang, X.; He, H.; Wang, S. *Biosens. Bioelectron.* **2018**, *118*, 174−180.
(22) Cao, A.; Zhang, C.-y. *Anal. Chem.* **2012**, *84*, 6199−6205.
(23) Guo, W.; Tian, Y.; Jiang, L. *Acc. Chem. Res.* **2013**, *46*, 2834−2846.
(24) Liu, H. L.; Jiang, Q. C.; Pang, J.; Jiang, Z. Y.; Cao, J.; Ji, L. N.; Xia, X. H.; Wang, K. *Adv. Funct. Mater.* **2018**, *28*, No. 1703847.
(25) Zhao, X. P.; Liu, F. F.; Hu, W. C.; Younis, M. R.; Wang, C.; Xia, X. H. *Anal. Chem.* **2019**, *91*, 3582−3589.
(26) Gao, P. C.; Hu, L. T.; Liu, N. N.; Yang, Z. K.; Lou, X. D.; Zhai, T. Y.; Li, H. Q.; Xia, F. *Adv. Mater.* **2016**, *28*, 460−465.
(27) Cheng, J.; Jiang, F.; Zhang, S. *Anal. Methods* **2021**, *13*, 1832−1838.
(28) Zhang, S.; Li, K.-B.; Pan, Y.; Han, D.-M. *Talanta* **2020**, *220*, No. 121420.
(29) Wang, Y.; Zhang, S.; Yan, H.; Quan, J.; Yang, L.; Chen, X.; Toimil-Molares, M. E.; Trautmann, C.; Li, H. *Anal. Chem.* **2021**, *93*, 6145−6150.
(30) Xiao, P.-P.; Wan, Q.-Q.; Liao, T.; Tu, J.-Y.; Zhang, G.-J.; Sun, Z.-Y. *Anal. Chem.* **2021**, *93*, 10966−10973.
(31) Liu, N. N.; Jiang, Y. N.; Zhou, Y. H.; Xia, F.; Guo, W.; Jiang, L. *Angew. Chem., Int. Ed.* **2013**, *52*, 2007−2011.
(32) Guo, W.; Hong, F.; Liu, N. N.; Huang, J. Y.; Wang, B. Y.; Duan, R. X.; Lou, X. D.; Xia, F. *Adv. Mater.* **2015**, *27*, 2090−2095.
(33) Liao, T.; Li, X.; Tong, Q.; Zou, K.; Zhang, H.; Tang, L.; Sun, Z.; Zhang, G.-J. *Anal. Chem.* **2017**, *89*, 5511−5518.
(34) Xie, Z.; Lei, J.; Yang, M.; Li, Y.; Geng, X.; Liu, S.; Wang, J. *Biosens. Bioelectron.* **2019**, *127*, 200−206.
(35) Xie, Z.; Yang, M.; Luo, L.; Lv, Y.; Song, K.; Liu, S.; Chen, D.; Wang, J. *Talanta* **2020**, *219*, No. 121213.
(36) Zhang, S.; Cheng, J.; Shi, W.; Li, K.-B.; Han, D.-M.; Xu, J.-J. *Anal. Chem.* **2020**, *92*, 5952−5959.
(37) Yang, L.; Liu, C.; Ren, W.; Li, Z. *ACS Appl. Mater. Interfaces* **2012**, *4*, 6450−6453.

https://doi.org/10.1021/acs.analchem.1c05332
Anal. Chem. 2022, 94, 4407−4416